



Published in final edited form as:

Angew Chem Int Ed Engl. 2010 September 24; 49(40): 7266–7270. doi:10.1002/anie.201003445.

Ligand-clustered “patchy” nanoparticles for modulated cellular uptake and in vivo tumor targeting

Zhiyong Poon^{*}, Shujun Chen[†], Amanda C Engler[†], Hyung'il Lee[†], Evrim Atas[§], Geoffrey von Maltzahn[‡], Sangeeta N Bhatia[‡], and Paula T Hammond[†]

^{*}Department of Materials Science and Engineering, Massachusetts Institute of Technology, Cambridge, Massachusetts 02139, USA

[†]Department of Chemical Engineering, Massachusetts Institute of Technology, Cambridge, Massachusetts 02139, USA

[‡]Harvard-MIT Division of Health Sciences and Technology, Massachusetts Institute of Technology, Cambridge, Massachusetts 02139, USA

[§]Department of Biomedical Engineering, Boston University, Boston, Massachusetts, 02215, USA

Abstract

Despite the evident success of using a multivalent approach to increase efficacy of targeted delivery, a clear understanding of how multiple ligands behave collectively to influence the uptake of nanoparticle cell-targeting agents has not been reached. Although when present in large quantity, multivalent ligands can increase binding avidities to cells, it is also conceivable, that the manner in which these ligands are presented to the cell may have a significant effect on uptake. Here we examine this parameter using a linear dendritic polymer construct that enabled us to pattern the surfaces of nanoparticles with variable sized ligand clusters in different spatial arrangements. We demonstrate for the first time the clear impact of folate presentation on intracellular uptake both in vitro and in vivo. The findings presented here suggest that the nature of ligand presentation on a nanoparticle surface may play an important role in drug targeting; the results suggest potential impact for other targeting moieties and provide a framework for further refinement of future multivalent targeting strategies.

Many biological systems interact through multiple simultaneous interactions^[1–3]. While it is well acknowledged that, on the macroscale, these multivalent interactions strongly influence ligand-receptor binding kinetics and the biological responses they govern, the microscale patterning of ligands on substrates can also have a profound effect on multivalent kinetics and are able to further modulate biological signaling^[4]. In particular, ligand-receptor clusters can dramatically increase interactions between cell and substrate; not only the valency, but spatial factors such as branching mode and the localized clustering of groups are important^[5–7] in influencing binding and downstream signaling processes^[8, 9]. Still, despite the prevalence of patterned ligand presentation in cell biology and its demonstrated significance on 2D tissue engineering formats^[10, 11], it remains largely unappreciated by those who design nanoparticle synthetic systems intended to interact with cells.

Traditionally, ligands have been attached in moderate to large quantities to liposomes, inorganic nanoparticles and linear-linear block copolymer micelles^[12, 13]; however, typically they are presented in a randomly distributed fashion across the nanoparticle surface

from a linear tether, typically polyethylene glycol (PEG), in a structure that does not enable manipulation of ligands in specific groupings with control of cluster group size and spacing. We hypothesized that precise control over the elements promoting and controlling multivalent presentation on targeted therapeutic carriers could enhance the efficacy and specificity of targeted delivery. To test this hypothesis, scaffolds that are able to localize a variable number of ligands within confined regions are required; this requirement cannot be satisfied by traditional material systems used in targeted delivery^[14] such as linear-linear block polymers and PEG-functional liposomes. Here we introduce the use of a systematic and informed linear dendritic design for a new modular polymer delivery system that can generate clustered or patchy presentations of ligand on micellar surfaces^[15]. We demonstrate the use of pre-functionalized linear dendritic polymers (LDPs) in forming mixed micelle formulations that present different spatial arrangements of variable sized ligand clusters and examine the targeting efficacy of these formulations in vitro and in vivo.

The design of the LDP is based on drug delivery principles, and each component is either fully biodegradable or biocompatible (Figure 1a). Hydrophobic PBLA (poly-benzyl-L-aspartate) forms the polypeptide linear block to which a generation four hydrolytically degradable polyester dendron is attached. The sixteen end branches of the dendron are extended with sixteen short hydrophilic PEG chains. The well-characterized model ligand folate^[16], which is conjugated to the free PEG end via NCC/NHS chemistries, was selected for this study. A range of folate functionalization on the dendron was confirmed by both ¹HNMR and UV-Vis, which allows the expression of different folate cluster size ranges on the micelle surface (Figure 2a, Supplemental Figure 1, 2a, 2c). The ability of the LDP system to form mixed micelles was confirmed by TEM and FRET, and this information is given in the supplementary information (Supplemental Figure 2d). TEM analysis using Fe³⁺ in the place of folate allow visualization of groupings of 'ligands' on the surface of the micelle (Figure 2b).

To investigate the influence of ligand clustering on receptor mediated uptake, a series of eight micelle formulations were used: 0%F-100%mix, the untargeted control containing unfunctionalized LDP (0%F) used as 100% of the micelle and 10%F-100%mix, 20%F-60%mix, 30%F-40%mix, 40%F-30%mix, 60%F-20%, 70%F-20%mix and 100%F-10%mix are formulations presenting a similar amount of folate in total. UV-Vis data show statistically similar numbers of folate per micelle by one way ANOVA analysis between the different groups at the 95% confidence interval (Figure 2c). We used FR overexpressing KB cells to evaluate targeting and binding of the micelles to receptors on the cell surface. After a 24 h period of incubation, the highest cell associated fluorescence was observed for cells incubated with the 20%F-60%mix formulation (Figure 3a). The measured EC50 (concentration producing 50% binding) was observed to be the lowest for the 20%F-60%mix micelle. To facilitate discussion, we approximated the apparent dissociation constants of the tested micelles (K_D) by fitting the experimental data to a 1:1 binding model for site-specific binding. The apparent micelle K_D is given in Table 1. EC50 and K_D values are similar, indicating that there is a direct relationship between binding and the measured fluorescence. The measured dissociation rate constant (k_{off}) of the different micelles also show that the optimal 20%F-60%mix formulation had the longest dissociation time ($2 \times 10^{-5} \text{ s}^{-1}$) (Figure 2d, Table 1). To examine the apparent rate of association (K_{on}) relationship between the micelles, we used the following equation: $k_{on} = k_{off}/K_D$ and found that the calculated values were not significantly different (less than 1 order of magnitude apart, Table 1). Confocal analysis and competitive binding experiments confirmed that our observations for binding and targeting are FR mediated and that the mechanism for internalization of targeted LDP is dependent on both energy driven endocytosis and the presence of folate receptors (Supplemental Figure 5).

To further account for the observed differences in cell targeting, we examined the rate of change of cell associated fluorescence post incubation with micelles as a measure of the kinetics of internalization via the folate receptor (Figure 3b). After a 1 h binding time for internalization, the rate of change in cell-associated fluorescence is not significantly different for all formulations between 1 h and 6 h, indicating that the actual mechanisms of folate internalization are not dependent on ligand presentation; however, the relative levels of cell fluorescence show a strong relationship with their respective binding avidities. All micelle formulations exhibited saturation uptake kinetics at longer time points, suggesting an equilibrium between uptake and secretion was reached by 20 h (Supplementary Figure 5c). These observations indicate that the enhanced cell targeting of micelles with optimal folate cluster presentation is attributed to having more micelles bind for longer residence times on the cell surface, which increases the chance for endocytosis.

We estimate that the dendritic element of the LDP has a head group area of ~50 to 80 nm² and the FR is a protein of ~30 kDa that projects a binding area of ~13 nm² into extra-cellular space^[17]. Examinations of cell membranes that overexpress FR indicate that the FR molecules exist in nanoscale clusters on lipid rafts, with a majority of those clusters consisting of 3 or more FR molecules^[18–22]. Given the available binding space afforded by each dendron, the range of folate-FR interactions that can occur is between 0–6, corresponding to LDP conjugated with up to 40% folate. If we were to treat each dendron as a binding entity, LDP-10%F (1.5 ± 0.4 folates/dendron) would bind most weakly to FR clusters and the binding energies of LDP-20%F (3.1 ± 0.9), LDP-30% (5.0 ± 0.9), and LDP-40%F (6.9 ± 0.9) would be greater. Once past the allowable number of ligand-receptor binding events (>LDP-50%F, 9.9±1.8 folates/dendron) within the binding space, the presence of excess ligands clustered in a small binding area would result in steric binding interference, lowering the binding energy^[23].

The cooperativity of this multivalent system can also be helpful in understanding binding effects. The LDP polymer is a negatively cooperative system, as $K_{\text{multivalent}} < (K_{\text{monovalent}})^{\alpha N}$, where K is the dissociation constant, N is the total number of ligands and α is the degree of cooperativity^[8] (Table 1). In negatively cooperative systems, each successive ligand interaction with a receptor is less favorable than the previous interaction. The calculated degree of cooperativity shows that all formulations were negatively cooperative ($\alpha < 1$ for all formulations), but among the tested micelles, 20%F-60%mix had the highest α , indicating that it is possible to achieve a particular ligand configuration that optimizes the use of each ligand, making the system less negatively cooperative (α closer to 1).

To investigate the significance of cluster presentation *in vivo*, we delivered formulations 0%F-100%mix, 20%F-60%mix, 60%F-20%mix and 70%F-20%mix (blood circulation half lives ~15–20 h Supplementary Figure 6) to nude mice bearing KB (FR+) and A375 (FR–) tumors. Figure 4 and Supplemental Figure 7 shows the results from imaging 48 h after injection of micelles. The highest normalized micelle fluorescence were observed for KB tumors in mice injected with 20%F-60%mix. Ratios for the untargeted formulations and all targeted formulations against A375 tumors were found to be within error. To further localize the micelles within the tumor tissue, flow cytometry analysis was performed on tumor cells isolated from whole tumors. We note that the similar trend in data for flow cytometry analysis and 3-D optical imaging show that at the 48 h time point, the majority of the fluorescence accounted for with tumor imaging were from micelles that have been internalized into tumor cells via specific (substantial) or non-specific mechanisms (minimal). The intravenously delivered targeted formulations were able to substantially internalize in live tumor cells *in vivo*, resulting in a higher population of cells with a higher fluorescence. Optimal clustering of folate also played an important role in enhancing

multivalent folate-FR cluster interactions, with the 20%F-60% mix formulation showing the highest level of fluorescence amongst targeted formulations ($P < 0.05$ for all analyses comparing 20%F-60% mix, 60%F-20% mix and 70%F-20% mix).

We have shown that ligand presentation is an important design parameter for increasing the efficacy of targeted nanoparticles. As discussed previously, the rates of endocytosis do not appear to be affected by ligand presentation. This finding, together with the observation that the rates of association (k_{on}) were similar for all formulations, support the conclusion that the enhanced uptake of optimized formulations are most likely dependent on their higher avidity and longer residence times on the cell membrane, which leads to a higher chance of endocytosis. This plays a critical role for in vivo targeting where the percentage of intravenously delivered nanoparticles that reach tumor sites via EPR (enhanced permeation and retention) is often less than 10 %ID/g^[24], resulting in a low concentration of nanoparticles in the tumor interstitial made available for uptake by tumor cells. To achieve substantial levels of therapy, the avidity of the delivered nanoparticle must be high enough to be able to bind to receptors under such conditions. The results presented here suggests that a shift in focus in molecularly targeted nanocarriers from ligand density to the specific manipulation of ligand cluster presentation may have important implications on cell targeting and can guide the development of more effective targeted delivery systems.

METHODS

Synthesis of LDP and its derivatives

We synthesized the LDP according to published protocols²². n-dodecyl-L-glutamate was substituted for benzyl-L-aspartic acid (Sigma Aldrich) and the synthesized polymer was characterized with ¹H NMR. Folate and labeling agents were conjugated to the LDP dendron using N-boc-1,3-diaminopropane (synthesized according to published protocols⁴⁶) as an intermediate. Detailed information on the synthesis and characterization of the polymer and the assembled micelles is provided in the Supplementary Information section online.

Synthesis of LDP and its derivatives

The LDP used in this study (PBLA₁₂-(Generation 4 dendron)Polyester-PEG(600 g/mol)) has a theoretical molecular weight of 14144 g/mol. For stoichiometric folate attachment to LDP, folic acid was activated using DCC/NHS chemistry and this was subsequently reacted with N-boc-1,3-diaminopropane. The resultant molecule (Folate-1,3-diaminopropane-boc) was deprotected with excess trifluoroacetic acid (10×) and purified by precipitation in water. After purification, folate-1,3-diaminopropane-NH₂ was reacted in stoichiometric excess with the amount of functional –COOH groups present on the LDP dendron (EDC/NHS) and in the presence of triethylamine to achieve folate functionalization of the dendron to varying percentages. All reactions were done in DMF. After reaction, the polymers were dialyzed in a 10KMWCO dialysis bag for 2 days before lyophilization to yield the product. We determined the degree of folate functionalization using UV-Vis (free folic acid as calibration, adsorption at 290nm) and ¹H NMR. We used the following peaks as reference: for folate, the aminobenzoyl moiety at ~6.5ppm (2H) and for LDP, the combined integration of 4.13ppm (d, 16H, –CH₂O) and 4.24–4.32ppm (m, 24H, –CH₂O) corresponding to the dendritic esters (40H). We chose the dendritic ester peaks as a reference because it is structurally closer to the position of folate on the molecule; these peaks were also used as a reference for ¹H NMR analysis during the synthesis of the LDP. N-boc-1,3-diaminopropane-DTPA (Sigma Aldrich) / VT680 (VisEn Medical) were also synthesized using DCC/NHS chemistry and subsequently deprotected to expose the second primary amine for reaction with activated (DCC/NHS) carboxyl PEG on the LDP. Alexa Fluor 488/594/ 647

(Invitrogen) cadaverine were directly labeled on the dendron with EDC/NHS chemistry. The labeling agents were conjugated at a 1:1 LDP:labeling agent molar ratio. After reaction, the products were separated with dialysis (10KMWCO) and purified with a Sephadex G-25 column before lyophilization. Labeled LDP were made by conjugating labeling agents to the dendron of unfunctionalized LDP. A small fixed amount (~5% concentration ratio) of the appropriate labeling LDP was used during self-assembly with the unfunctionalized and folate functionalized LDP to allow tracking of these particles (all conjugation schemes summarized in the methods section). This allows all micelle formulations to be labeled similarly with the dye. During assembly into nanoparticles, the hydrophobic PBLA linear block forms the core, which encapsulates hydrophobic drugs, while the hydrophilic dendritic block forms the shell, presenting folate that targets cell receptors. Self-assembly of these nanoparticles from pre-functionalized LDP enables variable sized folate clusters to be presented on the nanoparticle surface.

Micelle preparation and characterization

Folate conjugated LDP and non-functionalized LDP were mixed in different ratios to create nanoparticles with different folate spatial presentations. The micelles were further labeled either fluorescently or radioactively by incorporation of a small amount of the synthesized LDP-labeling agent; this ensures micelles contain on average a similar amount of fluorescent dye. Micelles containing LDP-DTPA were complexed with ^{111}In (InCl) or Fe^{3+} (FeCl_3) in sodium acetate buffer and were purified from the uncomplexed metal ions using a PD-10 salt column (GE healthcare). Micelles were self-assembled using a dialysis method: briefly, the LDP formulations (dissolved in DMF) were placed inside a 10KMWCO dialysis bag (Pierce Chemical) and dialyzed against DI water under sink conditions. DI water was replaced frequently for a total dialysis time of ~24 h. After all DMF was removed, the contents of the dialysis bags were filtered with a 0.2 μm teflon filter before lyophilization and use. Micelles were characterized using dynamic light scattering (CONTIN fit, ZetaPALS), TEM and FRET (AF488 and AF594 are donor-acceptor pairs). An excitation wavelength of 475 nm (AF488 donor excitation) was used and emission was recorded at 630 nm (AF594 acceptor emission). For TEM imaging, micelle solutions were drop-cast onto carbon coated copper grids without any staining. TEM of these micelles was performed on a JEOL 2011 high contrast digital TEM operating at 200KV accelerating voltage. The degree of folate conjugation on LDP was determined using UV-vis spectroscopy (absorption at 290nm). Free folic acid was used to obtain a standard calibration. Folate surface density was determined using aggregation numbers estimated from LDP (Materials Studio) and micelle dimensions. Addition of folate increased the diameters of the micelles and micelles with the same amount of folate have averaged diameters within $\pm 10\%$ of each another (Figure 2e). In addition, the zeta potentials of all micelle variations were also constant at $\sim -20 \pm 5$ mV (Supplementary Figure 3). This suggests that the aggregation numbers of the micelles do not change significantly, even when different polymer ratios are used in the formation of the micelles. We estimate that the aggregation numbers are in the order of 10^3 based on data from DLS/TEM and calculations of the size of each individual LDP from Materials Studio®. CMCs measured for all micelles were of the same order of magnitude of 10^{-8}M .

Radiolabeling

Formulations (1mg/mL) containing the LDP-DTPA polymer in PBS were incubated with 200 μCi of $^{111}\text{InCl}_3$ (in 1M sodium acetate buffer) at room temperature for 30 min. The resulting radiolabelled formulations were purified from free ^{111}In by gel filtration through a PD-10 column (GE healthcare) using PBS as the eluting phase.

In vitro experimentation

Human nasopharyngeal carcinoma cells (KB, FR positive)^{43,47} (ATCC), and human melanoma cells (A375, FR negative)⁴⁸ (ATCC), were used in our experiments. Folic acid free 1640 RPMI media was bought from Invitrogen, supplemented with 10% fetal bovine serum, 50 units/mL penicillin and 50 units/mL streptomycin. All cells were cultured in this media for at least 4 days before use. For all experiments, cells were scraped, washed, counted and plated as necessary in 24 or 96 well plates and allowed to grow to ~70% confluence. Before use, new media was added following a wash with PBS supplemented with 0.1% BSA. For determining uptake, micelle formulations (0.5mg/mL, AF647 labeled) were added for different incubation times. After incubation, the cells were washed with PBS ($\times 3$), trypsinized and re-suspended in PBS (0.1% BSA) for flow cytometry analysis. For binding avidity experiments, a range of micelle formulations at different concentrations were incubated with cells on ice for 1 h, washed with cold PBS to remove unbound ligand and re-suspended in cold PBS for flow cytometry analysis. Polymer concentrations used were above the CMC of 1×10^{-8} M. The degree of specific binding was determined by subtracting the amount of non-specific binding (micelle with no ligand) from total binding. To facilitate analysis, apparent K_D values were calculated by fitting experimental data to a non-linear regression method for a 1:1 single site specific binding model in PRISM (built in model). For dissociation kinetic experiments, cells were fixed in 4% paraformaldehyde, washed with PBS (0.1% BSA) and allowed to bind with micelles for 1 h to allow equilibrium. Following incubation, the cells were centrifuged and re-suspended in fresh buffer without micelles. This cell suspension was constantly stirred and was sampled at several time points thereafter to determine remaining cell fluorescence as a measure of the degree of dissociation of bound micelles. The sampled cells were spun down, washed, lysed and the resultant AF647 fluorescence from the lysed cells was measured using a spectrofluorometer. The decay in fluorescence was plotted against time and the experimental data was fitted to a built-in one phase exponential decay model in PRISM to determine apparent k_{off} values. As k_{off} and K_D were measured at different temperatures, the calculated rate of association (K_{on}) using equation: $k_{on} = k_{off}/K_D$, are also apparent values and are used to show the K_{on} relationship between different micelles. All flow cytometry analyses were performed on an LSR II (BD Biosciences) system.

For confocal microscopy, cells were grown until 50% confluent on chamber slides and treated with various micelle formulations and transferrin-A488 (when necessary) under different conditions (AF647 labeled). The cells were then washed repeatedly with PBS, fixed with 4% paraformaldehyde, permeabilized with cold ethanol, blocked with 0.1% BSA in PBS and stained with Hoechst (10 μ g/mL) for 5 min. The fixed cells were then washed again with PBS and examined with a Delta vision confocal microscope (60X).

In vivo experimentation

All in vivo experimentation was carried out under the supervision of the Division of Comparative Medicine, Massachusetts Institute of Technology, and in compliance with the Principles of Laboratory Animal Care of the National Institutes of Health.

Female nude BALB/c mice (3–4 weeks old, Charles River) were fed a folate deficient diet (Research Diets) for at least a week to achieve plasma folate levels commensurate with humans. Tumors were induced subcutaneously and bilaterally in the hind flanks with 2×10^6 KB/A375 cells. Experimentation began when the tumors developed to ~ 100 – 200 mm³ (<10% body weight, <1cm in any dimension). Tumor-bearing mice were then separated into random groups and given tail vein injections of labeled formulations (10 mg polymer/kg, 1 injection/formulation/mice). Blood circulation half-lives were determined by the decrease in radioactivity from blood drawn from the saphenous vein with heparinized capillary tubes. 3-

D fluorescence imaging was performed using an IVIS imaging system and mice to be imaged were given an injection of AngioSense750 (0.1mL/mice, 5nmol) 24hrs before imaging. VT680 fluorescence was detected using 675nm/720nm (ex/em) and AngioSense750 was detected using 745/800 (ex/em). For flow cytometry analyses of tumor cells, xenograft whole tumors were minced completely with sterile blades before a mixture of collagenase (II) in RPMI 1640 medium was added (200–250 units of collagenase/mL). The tumor pieces were allowed to incubate at 37°C for 3– 4 hrs with gentle agitation every 30min. At the end of the incubation, cells were filtered through a 0.45µm nylon mesh, washed with PBS (X3) and counter stained with propidium iodide (5µM), washed with PBS and re-suspended. VT680 micelle fluorescence was detected on the LSRII using the APC Cy7 detector.

Statistical Analysis

All values shown are in mean ± STD unless otherwise specified. Analyses were done by unpaired Student's t-test and one way ANOVA and considered significant at P<0.05.

Supplementary Material

Refer to Web version on PubMed Central for supplementary material.

Acknowledgments

This work was funded by the National Institute of Health, the MIT Center for Cancer Nanotechnology Excellence and the National Science Foundation. The authors wish to thank Glenn Paradise (MIT Koch Institute FACS facility) and Eliza Vasile (MIT Koch Institute Microscopy and Imaging facility). We also wish to thank the Institute of Soldier Nanotechnologies (ISN) and the Center for Material Science and Engineering (CMSE) for use of facilities and equipment.

REFERENCES

- [1]. Kitov PI, Sadowska JM, Mulvey G, Armstrong GD, Ling H, Pannu NS, Read RJ, Bundle DR. *Nature (London)*. 2000; 403:669. [PubMed: 10688205]
- [2]. Mourez M, Kane RS, Mogridge J, Metallo S, Deschatelets P, Sellman BR, Whitesides GM, Collier RJ. *Nat. Biotechnol.* 2001; 19:958. [PubMed: 11581662]
- [3]. Montet X, Funovics M, Montet-Abou K, Weissleder R, Josephson L. *J. Med. Chem.* 2006; 49:6087. [PubMed: 17004722]
- [4]. Cairo CW, Gestwicki JE, Kanai M, Kiessling LL. *J. Am. Chem. Soc.* 2002; 124:1615. [PubMed: 11853434]
- [5]. Andre S, Kaltner H, Furuike T, Nishimura SI, Gabius HJ. *Bioconjugate Chemistry*. 2004; 15:87. [PubMed: 14733587]
- [6]. Biessen EAL, Noorman F, van Teijlingen ME, Kuiper J, Barrett-Bergshoeff M, Bijsterbosch MK, Rijken DC, van Berkel TJ. *Journal of Biological Chemistry*. 1996; 271:28024. [PubMed: 8910412]
- [7]. David A, Kopeckova P, Minko T, Rubinstein A, Kopecek J. *European Journal of Cancer*. 2004; 40:148. [PubMed: 14687799]
- [8]. Mammen M, Chio S-K, Whitesides GM. *Angew. Chem., Int. Ed.* 1998; 37:2755.
- [9]. Schlessinger J. *Cell (Cambridge, Mass.)*. 2000; 103:211.
- [10]. Maheshwari G, Brown G, Lauffenburger DA, Wells A, Griffith LG. *J. Cell Sci.* 2000; 113:1677. [PubMed: 10769199]
- [11]. Koo LY, Irvine DJ, Mayes AM, Lauffenburger DA, Griffith LG. *J. Cell Sci.* 2002; 115:1423. [PubMed: 11896190]
- [12]. Azarmi S, Roa WH, Lobenberg R. *Adv. Drug Delivery Rev.* 2008; 60:863.
- [13]. Duncan R. *Nat. Rev. Cancer*. 2006; 6:688. [PubMed: 16900224]

- [14]. Duncan R. *Nat. Rev. Drug Discovery*. 2003; 2:347.
- [15]. Tian L, Hammond PT. *Chem. Mater.* 2006; 18:3976.
- [16]. Salazar MDA, Ratnam M. *Cancer Metastasis Rev.* 2007; 26:141. [PubMed: 17333345]
- [17]. Holm J, Hansen SI, Hoier-Madsen M, Birn H, Helkjaer P-E. *Arch. Biochem. Biophys.* 1999; 366:183. [PubMed: 10356282]
- [18]. Weitman SD, Lark RH, Coney LR, Fort DW, Frasca V, Zurawski VR Jr, Kamen BA. *Cancer Res.* 1992; 52:3396. [PubMed: 1596899]
- [19]. Turek JJ, Leamon CP, Low PS. *J. Cell Sci.* 1993; 106:423. [PubMed: 8270640]
- [20]. Kamen BA, Wang MT, Streckfuss AJ, Peryea X, Anderson RGW. *J. Biol. Chem.* 1988; 263:13602. [PubMed: 3417674]
- [21]. Lee RJ, Low PS. *J. Biol. Chem.* 1994; 269:3198. [PubMed: 8106354]
- [22]. Hong S, Leroueil PR, Majoros IJ, Orr BG, Baker JR, Banaszak Holl MM. *Chem. Biol.* (Cambridge, MA, U. S.). 2007; 14:107.
- [23]. Hlavacek WS, Posner RG, Perelson AS. *Biophys. J.* 1999; 76:3031. [PubMed: 10354429]
- [24]. Maeda H, Wu J, Sawa T, Matsumura Y, Hori K. *J. Controlled Release.* 2000; 65:271.

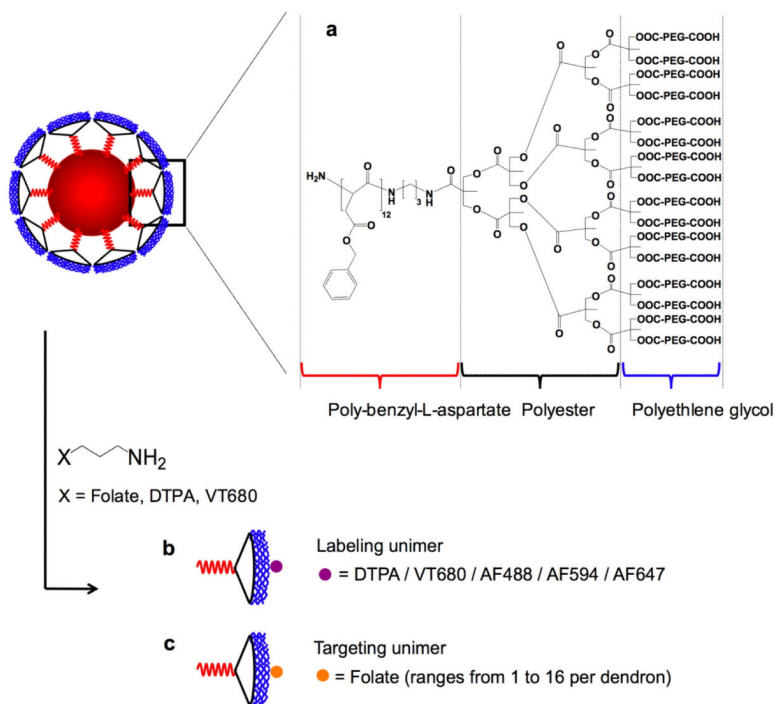


Figure 1. Chemical structure and self-assembly of linear dendritic polymers (LDP). a) Detailed chemical structure of the LDP and illustration of its self-assembly (PBLA= poly(benzyl-L-aspartic acid), PED=polyester dendron, PEG=poly(ethylene glycol)). b) Labeling LDP used in our study. Labeling schemes are described in methods. c) Folate conjugated to dendron of LDP at various percentages. Conjugation chemistry is described in methods.

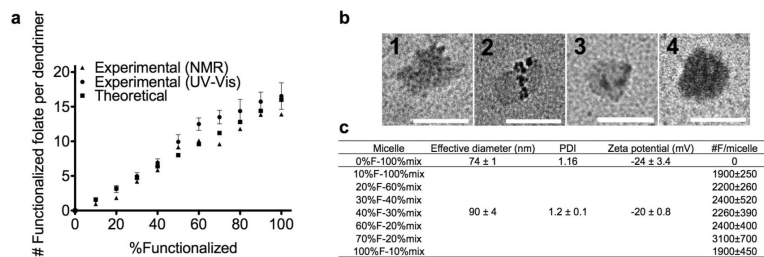
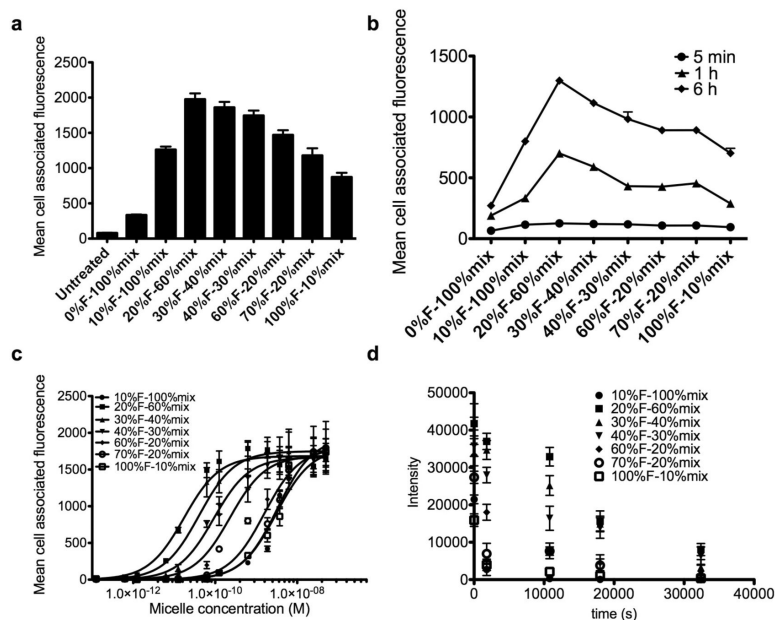


Figure 2. Characterization of LDP mixed micelle system. a) Theoretical vs experimental degree of conjugation to dendron. Experimental values for UV-Vis were calculated using at least 3 independent sets of measurements (mean±STD) with free folic acid as the calibration. ¹HNMR quantification is described in methods. b) TEM images of representative formulations are shown. Clusters of DTPA-Fe³⁺ on the micelle surface show the formation of mixed micelles. Scale bar = 100 nm. Formulations 10%F-100% mix (1), 20%F-60% mix (2), 30%F-40% mix (3) and 30%F-100% mix (4) are shown. c) Summary of the eight micelle formulations used in this study. 0%F-100% mix is the untargeted control, all other formulations present similar amounts (not statistically different by one way ANOVA analysis at the 95% CI) of folate but in different cluster size and arrangements. Total number of folate presented per micelle (mean±STD) is calculated based on at least 3 sets of data (UV-Vis) using an approximate micelle aggregation number of 1000 (based on measured diameters and estimates of LDP unimer dimensions from Materials Studio). Average micelle diameters and zeta potentials are given in mean±STD of the averages of at least 10 individual measurements per micelle. Additional information on diameter, zeta potential information and folate presentation are shown in Supplementary Figure 3 and 2b.

**Figure 3.**

In vitro evaluation of patchy micelles on KB (folate receptor, FR+) and A375 (FR-) cells. a) KB cell associated fluorescence after 24 h of incubation with micelle formulations. Highest fluorescence was measured from KB cells incubated with 20%F-60% mix formulation (Supplementary 4a). b) Measured cell associated fluorescence of KB cells at 5 min, 1 h and 6 h post incubation. Increase in cell associated fluorescence between 1 h and 6 h are similar for all targeted formulations, indicating that rate of endocytosis is unaffected by folate presentation. c) The binding avidity (K_D) measured for targeted formulations show highest avidity with 20%F-60% mix. d) The measured rate of decrease in micelle fluorescence after fixed KB cells pre-incubated to equilibrium with micelles was re-suspended in PBS. Non-linear regression analysis using a one phase exponential decay model gives the apparent dissociation rate constant of micelles from membrane receptors (k_{off}). Calculated values for targeted formulations show longest dissociation rate constant with 20%F-60% mix. K_D , k_{off} and k_{on} values are shown in Table 1. All graphs shown are made with measurements on $n > 3$ independent experiments and are given in mean \pm SEM values. Individual flow cytometry measurements were averaged out of 10000 events.

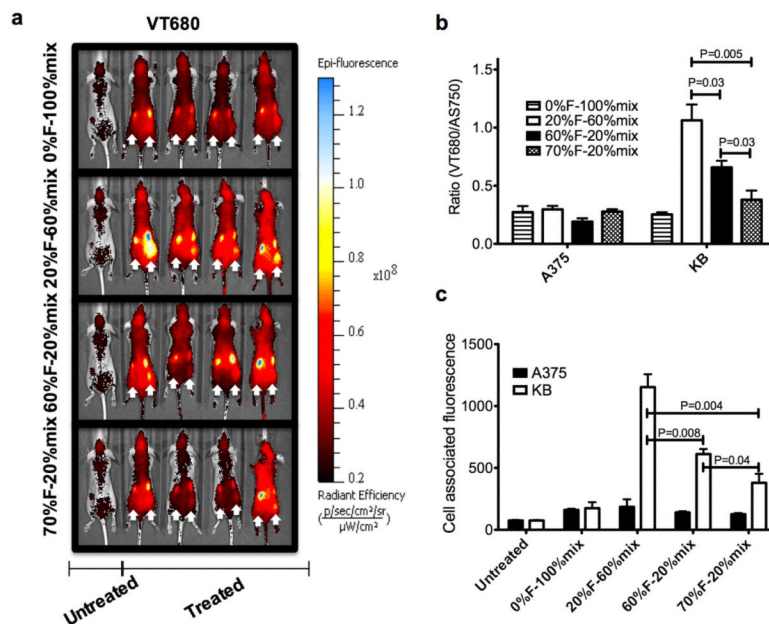


Figure 4.

In vivo evaluation of patchy micelles on nude mice bearing two different tumors (Right flank: KB, Left flank: A375). a) Fluorescence 3-D optical imaging of tumored nude mice 48h after injection with different formulation micelles. Micelle fluorescence (VT680) from tumors on both flanks are indicated by the arrows. A side by side comparison of VT680 and AngioSense750 fluorescence is also shown in Supplementary Figure 7 to allow identification of the tumors. b) Normalized tumor fluorescence (VivoTag680(VT680)/AngioSense750(AS750)) of tumors ($n = 4$) showing the highest in vivo targeting with 20%F-60%mix micelles. Raw fluorescence data is an average of the fluorescence in the region of interest, given in units of efficiency. Ratios are 0.27 ± 0.11 , 0.30 ± 0.06 , 0.19 ± 0.06 and 0.28 ± 0.04 for A375 tumors and 0.25 ± 0.04 , 1.06 ± 0.27 , 0.66 ± 0.11 and 0.38 ± 0.16 for KB tumors (0%F-100%mix, 20%F-60%mix, 60%F-20%mix and 70%F-20%mix respectively). c) Average cell associated micelle fluorescence for cells gated in Q1+Q3 (see Supplemental Figure 7) are 160 ± 16 , 185 ± 104 , 140 ± 17 and 126 ± 15 for A375 tumors and 175 ± 84 , 1153 ± 104 , 611 ± 71 and 380 ± 126 for KB tumors (0%F-100%mix, 20%F-60%mix, 60%F-20%mix and 70%F-20%mix respectively). All data is given in mean \pm SEM.

Table 1

Apparent K_D , k_{on} and k_{off} values for the targeted formulations. K_D and k_{off} were determined experimentally (at least 3 sets of independent data each), K_{on} was calculated as $k_{on} = k_{off}/K_D$ using mean k_{off} and K_D values.

Micelle	K_D (M)	K_{off} (s^{-1})	K_{on} ($M^{-1}s^{-1}$)
10%F–100%mix	(3.1±0.5) E-09	(1.2±0.3) E-03	3.8E+05
20%F–60%mix	(1.7±0.3) E-11	(1.6±0.4) E-05	9.6E+05
30%F–40%mix	(4.0±1.2) E-11	(3.0±1.8) E-05	7.4E+05
40%F–30%mix	(9.2±1.8) E-11	(8.3±0.3) E-05	9.0E+05
60%F–20%mix	(2.3±0.8) E-10	(4.0±1.2) E-04	1.8E+06
70%F–20%mix	(1.5±0.8) E-10	(1.2±0.7) E-03	7.4E+05
100%F–10%mix	(3.3±0.6) E-09	(9.3±1.9) E-04	2.8E+05